Advanced Steel Construction – Vol. 18 No. 1 (2022) 506–516
DOI:10.18057/IJASC.2022.18.1.9

EXPERIMENTAL AND NUMERICAL INVESTIGATION ON SEISMIC PERFORMANCE OF RING-BEAM CONNECTION TO GANGUE CONCRETE FILLED STEEL TUBULAR COLUMNS

Chen Fang [1], Guo-Chang Li [2], Lei Zhang [3, 4, *] and Zhi-Jian Yang [2]

[1] *Midwest Roadside Safety Facility, University of Nebraska-Lincoln, Lincoln, Nebraska 68583, USA*
[2] *School of Civil Engineering, Shenyang Jianzhu University, Shenyang, Liaoning 110168, China*
[3] *Lecturer, Department of Civil Engineering and Architecture, Jiangsu University of Science and Technology, Zhenjiang, Jiangsu 212100, China*
[4] *Postdoctor, Institute of Geotechnical Engineering, Nanjing Tech University, Nanjing, Jiangsu 211816, China*
** (Corresponding author: E-mail: lei.zhang@just.edu.cn)*

ABSTRACT

This paper presents an investigation on seismic performance of a ring-beam connection that is used to connect reinforced gangue concrete (RGC) beam to coal-gangue concrete-filled steel tubular (GCFST) column. Two specimens, including an interior connection with two beams and an exterior connection with one beam, were designed and fabricated for experimental tests under full-reversing cyclic loads at beam ends. In addition, finite element models which corresponded to tested specimens were developed using ABAQUS to conduct numerical simulations of the composite connection subjected to the combined axial and cyclic loads. The feasibility of the developed model to predict failure modes and load-deformation response of the connection was validated by comparing with test results. The response of the ring-beam connection to cyclic loads was examined with respects to the load-bearing capacity, deformation resistance, stiffness and strength degradation, ability to dissipate energy in a seismic event, and ductility. With numerical models, parametric analysis was completed to evaluate the influences of material and structural parameters on connection resistance against cyclic loads. Based on the results of parametric studies, a restoring force model of skeleton curve for the ring-beam connection was developed in terms of ultimate capacity and corresponding deformation. The results provided practical suggestions for the application of ring-beam connection to GCFST column in the projects.

ARTICLE HISTORY

Received: 14 October 2020
Revised: 1 July 2021
Accepted: 4 July 2021

KEYWORDS

Column-beam connection;
Gangue concrete filled steel tube;
Ring-beam connection;
Seismic behavior;
Finite element analysis;
Full-scale test

1. Introduction

Coal-gangue concrete filled steel tubular (GCFST) structure is an innovative composite structure adoptable for the high-rise buildings and bridges [1]. Gangue concrete filled steel tubular structural element is designed to consist of a steel tube and gangue concrete filled in the tube. This composite structure takes advantages of steel tube and confined coal-gangue concrete. The confinement created by steel tube could significantly increase concrete strength, and the coal-gangue concrete filled in the tube provides supplementary resistance against tube buckling [2; 3]. GCFST structure exhibits benefits to achieve high strength and large ductility under cyclic loading. Furthermore, prominent merits can be found for the GCFST structures. Compared to regular concrete, the coal-gangue concrete has the superior lateral deformation resistance, resulting in the full use of the tube confinement effects and futher improve the capacity of the composite structure [4]. Another advantage which attracts the interests of researchers and designers is its less weight than the concrete filled steel tubular (CFST) structure due to the less density of gangue concrete. With the development of the society, it is a trend to develop the green building in Civil Engineering [5]. As a non-recyclable industrial waste, the use of the gangue for building construction is an economic approach to reduce environmental pollution and achieve the social benefits [6].

In the seismic design principle, a column-to-beam connection is a critical element that determines the integrity and safety of the frame building. The column-beam connection provides stiffness and strength for a building to ensure its integrity under an earthquake. Many structures collapsed due to severe damage to the column-beam connection under various earthquake events [7] such as Wenchuan in China [8]. Therefore, the strength and ductility of the column-to-beam connection should be improved to ensure the stability and safety of the entire building under earthquake events.

Many scholars and designers have conducted a series of studies on performance of various connections between CFST column and beam. Goldsworthy and Gardner [9] completed an experimental study that proposed a CFST column-to-beam connection and investigated its performance under wind or seismic loading. Kataoka et al. [10] developed a new connection between CFST column and steel beam using endplates and bolts and conducted experimental investigations on the dynamic behaviors. The study also carried out an analytical evaluation for the connection behavior based on ABNT NBR 8800. Agheshlui et al. [11] investigated the cyclic behavior of moment-resisting bolted connection between square CFST column and steel beams. The study analyzed the failure mode, hysteretic performance, capacity, stiffness of proposed connection and demonstrated its satisfactory performance to resist lateral loads for high-rise building. Tizani et al. [12] designed a new connection to CFST columns using the blind bolts and experimentally examined the performance and reliability of this new connection for the seismic design requirements. The study indicated that this new connection with an acceptable capacity to dissipate energy has adequate seismic resistance for the entire building. Khanouki et al. [13] created ABAQUS numerical model of a through-beam connection to CFST column and evaluated its cyclic behaviors using a series of parametric studies. Choi et al. [14] developed a through-type CFST column-to-beam connection and experimentally studied its failure mode and energy-dissipation capacity for earthquake-resistant applications. However, limited studies have been conducted to investigate the cyclic-loaded response of the GCFST column-to-beam connection. Due to inadequate understanding of seismic behavior, this new composite connection does not reach its full potential in the application, and more studies need to provide information on the performance of the promising composite connection for design and application in the engineering projects.

This paper proposed and designed a ring-beam connection that is used to connect RGC beams with GCFST column. The connection specimens were fabricated for experimental tests to investigate their seismic behaviors. In addition, finite element models corresponding to experimental specimens were developed using ABAQUS, and the feasibility of the developed model was verified by comparing numerical results with test data. Several critical indexes were examined to evaluate the connection performance in a seismic event for this study. Parametric analysis was conducted to examine the influences of concrete and structural parameters on the connection response. Finally, a restoring force model of skeleton curve for the ring-beam connection was developed in terms of ultimate capacity and corresponding deformation.

2. Experimental tests

2.1. Experimental specimens

The prototype of the ring-beam connection was designed in accordance with requirements of the code CECS28-2012 [15]. The ring-beam connection to GCFST column was fabricated in structural laboratory at the Shenyang Jianzhu University. Fig. 1 shows the geometries and reinforcement details of tested specimen. This composite connection consisted of a GCFST column, RGC beams of a frame building, an RGC ring beam and shear rings. The shear ring was designed as circle reinforcing bars which was welded to tube wall in the vicinity of ring beam bottom and embedded in the ring beam. The function of welded shear ring was to transfer shear stress from ring beam to GCFST

column. The number of shear ring was determined from shear stress generated by cyclic loads and design requirement provided in GB50936-2014. For the experimental program, two specimens were tested: one interior connection that includes two frame beams and one exterior connection involving one frame beam. The column was designed as a circular gangue concrete filled steel tubular column with a diameter of 325 mm. The thickness of steel tube was 6 mm, which results in a steel ratio of 0.078 for the GCFST column. The clear height of the GCFST column was 1500 mm. All beams with cross-sectional dimensions of 180×250 mm were reinforced by 2Φ20 longitudinal bars and Φ10 hoops spaced at 100 mm. The ring beam was 120 mm in width and 250 mm in depth. The ring beam was reinforced using 2Φ12 longitudinal bars and Φ6 hoops spaced at 100 mm. An axial load, which produces an axial load ratio of 0.6, was placed at the top column during the process of test.

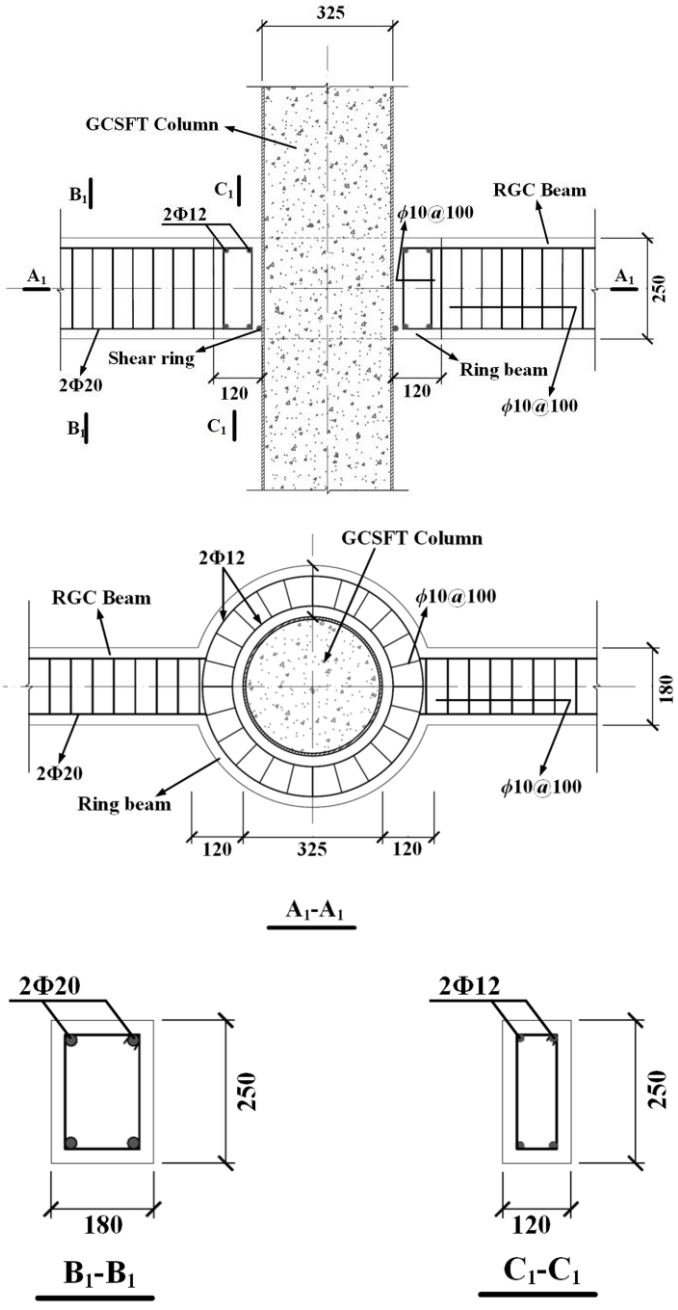

Fig. 1 Geometries and reinforcement details of tested specimen

Table 1 lists the geometries and reinforcement details of the tested connections. In this table, *D* is the outside diameter of GCFST column; *t* is the thickness of steel tube; *b* and *h* are the width and depth of the frame beam, respectively; *H* is column height; *L* is the frame beam length; A_{sf} is the area of longitudinal reinforcement for frame beam; *h'* is ring beam height; A_{sr} is the area of circle reinforcement for ring beam; *b'* is the width of the ring beam; *n* is the axial load ratio for the GCFST column [15].

Table 1
Dimensions of tested specimens

Specimen	*D*×*t* (mm)	*H* (m)	*L* (m)	*b* (m)	*h* (m)	A_{sf}	*b'* (m)	A_{sr}	hoop	*n*
JH-E-B	325×6	1.5	1	0.18	0.25	2Φ20	0.12	2Φ12	Φ10	0.6
JH-E-Z	325×6	1.5	2	0.18	0.25	2Φ20	0.12	2Φ12	Φ10	0.6

Based on the design code GB50011-2010 [16], the specimens were designed in accordance with the philosophy that "strong column and weak beam". Therefore, the RGC frame beam was designed to fail under earthquake events, while the column must have sufficient strength to resist the earthquake. This principle can ensure safety and stability of a building under earthquake events. Fig. 2 shows the tested specimen of JH-E-Z connection.

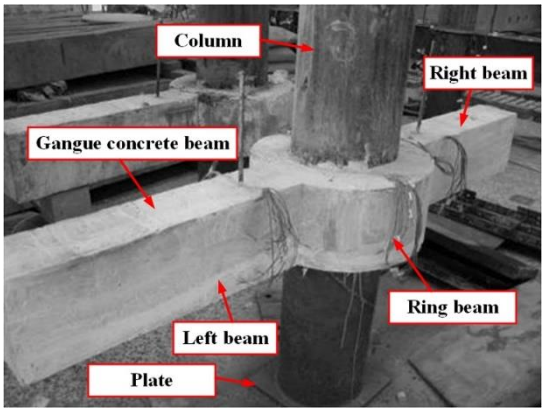

Fig. 2 Tested specimen of JH-E-Z connection

2.2. Concrete and steel properties

Tension test was conducted on the steel coupon to measure the steel properties using the code GB/T228-2002 (2003) [17]. The steel had the yield strength of 500 MPa, the ultimate strength of 650 MPa, and the Young's modulus of 215 GPa. Table 2 lists the material properties for each steel determined for this experimental investigation. Gangue concrete mix proportion that was designed by the weight included, the cement: 420 kg/m^3; sand: 412.5 kg/m^3; gangue: 412.5 kg/m^3; water: 250 kg/m^3; and coarse aggregate: 608 kg/m^3. The regular Portland cement with a grade of 32.5 and the coal gangue with an aggregate size of 5~10 mm collected in Fuxin city were used to produce the gangue concrete. The compressive cube strength test was performed on the gangue concrete block at 28 days according to GB/T50081-2002 (2003) [18]. The average strength of the coal-gangue concrete was 21.4 MPa.

Table 2
Steel material properties

Steel	f_y (MPa)	f_u (MPa)	*E* (MPa)
Φ20	500	650	2.17×10^5
Φ12	385	553	2.07×10^5
Φ10	325	427	2.06×10^5
Φ6	342	398	2.15×10^5
Steel tube	324	459	2.19×10^5

2.3. Test preparation

Fig. 3 illustrates experimental setup. A constant axial load (N_0) created using a hydraulic jack was imposed at the top of the GCFST column. The top and bottom of the column were restrained to the hinged boundary conditions. Two MTS hydraulic rams were set at both ends of RGC beams to generate a cyclic load. In the initial stage, the axial load was gradually increased up to the designed load prior to the cyclic load. The axial load was employed to simulate the dead load effects.

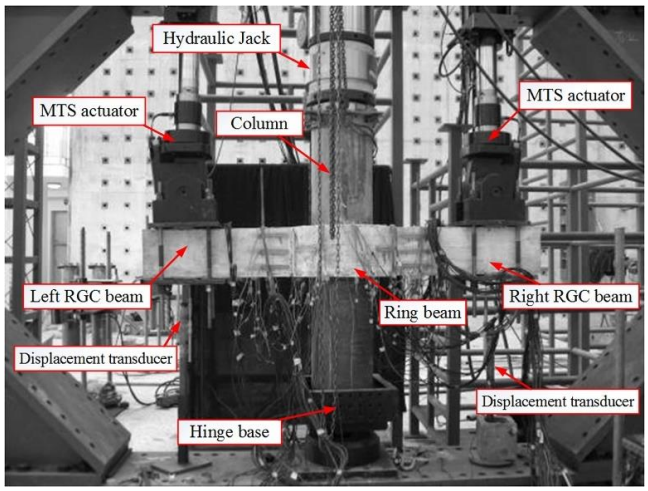

Fig. 3 Test setup

The cyclic load determined based on JGJ/T101-2015 [19] was applied at beam ends within two stages as shown in Fig. 4. At the force control stage, two cycles were employed using the load levels of $0.25P_y$, $0.50P_y$, $0.75P_y$ and $1.0P_y$ in both beam ends, where P_y is the estimated connection yield load under combined axial and cyclic loads and received from finite element models. In these specimens, P_y was close to the yield strength of RGC beam. As the cyclic load reached Py, the connection was determined to be yielded, and then the displace control was used to apply the cyclic loads. At the displacement control stage, displacement cycles with an increase rate of Δ_y were applied at the GRC beam ends, in which Δ_y represents the displacement obtained at P_y. Each displacement level had three displacement cycles before failure of the ring-beam connection. In the test, a 1-kN/s force rate was used at the force-control stage, and a 1-mm/s displacement rate was utilized at the displacement-control stage.

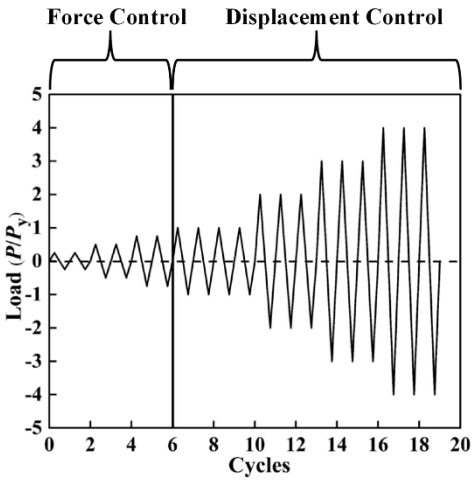

Fig. 4 Applied cyclic loading stage

The connection response was recorded and examined in the terms of the displacement of GCFST column, displacement and load at beam end, strains of concrete and reinforcing bars. Loads at both beam ends were measured using the transducers of MTS hydraulic actuators, and displacements were recorded using displacement transducers located below RCC beams. A displacement transducer was set at the top of the GCFST column to receive the column displacement. The dispacements at the RGC beams were recorded using two displacement transducers. strains for the steel tube, reinforcing bars, and coal-gangue concrete were obtained using several strain gauges. The locations of these displacement transducers are shown in Fig. 3.

2.4. Experimental observations

2.4.1. JH6-E-Z specimen

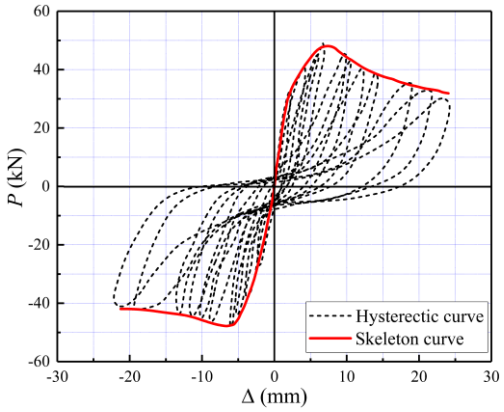

Fig. 5 Load-displacement curve for JH-E-Z connection

Fig. 5 illustrates the load-displacement time history for JH-E-Z connection. As shown in this figure, the specimen deformation demonstrated the linear characteristics at the beginning of testing, and cracking did not occur to the connection. When the cyclic force in the beams ends reached 13 kN, the first crack was observed at the end of the frame beam in the vicinity of ring beam. The 0.05 mm wide first crack was perpendicular to RGC frame beam. As the cyclic load increased to 19 kN, the concrete cracks were 0.1 mm in width and shown at the ring beam bottom. Concrete cracking was developed along the radial direction of ring beam. With the increased cyclic load, the vertical cracks and the diagonal cracks were shown in the side of ring beam. Diagonal cracks were propagated from the junction between ring beam and frame beam to the ring beam side as the cyclic load approached to 24 kN. It was clear that a wide crack along the beam depth was observed in the junction between the ring beam and the frame beam. This specimen was yielded at this load. After the yield load, the displacement control was used to impose the cyclic displacement in both beam ends. When the cyclic displacement increased to $2\Delta_y$, the composite connection reached its ultimate load bearing capacity. As the cyclic displacement increased, new cracks were created on the sides of the ring beam and the frame beam. At the cyclic displacement of $5\Delta_y$, the ring beam experienced significant concrete spalling, with the formation of lantern-shaped cracks in the ring beam side. The reinforcing bars of the connection were exposed. Failure modes of the specimen JH6-E-Z were shown in Fig. 6.

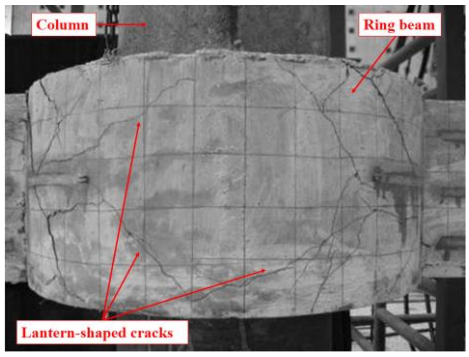

(a) Front side

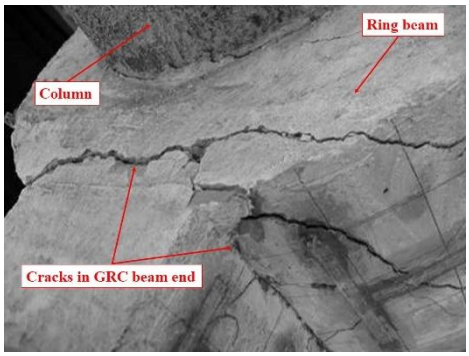

(b) Top side

Fig. 6 Failure mode for JH-E-Z connection

2.4.2. JH6-E-B specimen

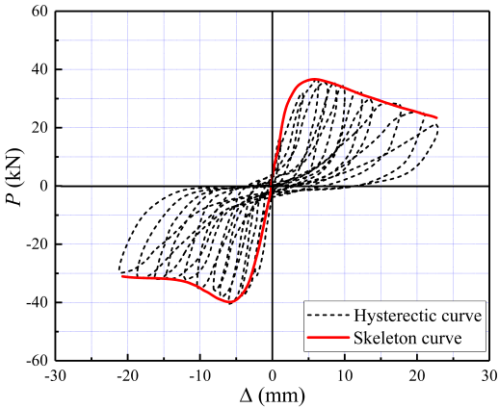

Fig. 7 Load-displacement curve for JH-E-B connection

Fig. 7 shows load-displacement time history for JH-E-B connection. The composite connection showed an elastic behavior, and the crack was not observed when the cyclic load was less than 10 kN at the force control phase. When the cyclic load increased to 11 kN, first vertical crack was noted at the ends of the frame beams. The width of the first crack was measured about 0.05 mm. The crack in the frame beam was developed to diagonal cracks from the beam bottom when the connection was subjected to cyclic load of 16 kN. These cracks were approximately 0.1 mm in width. The increase in the cyclic load resulted in the development of new cracks in the beam sides and the propagation of diagonal cracks to the ring beam side. A wide crack through the frame beam height was generated in the frame beam region that was close to ring beam at a cyclic load of 21 kN. This load was regarded as the yield load for this connection specimen. The displacement at the yield load was specified as the yield displacement for this connection specimen. After the yield load, the test was transferred to be at the displacement control phase. The existing cracks were increased and widened with the increase in the cyclic displacement. At the cyclic displacement of $2\Delta_y$, a plastic hinge was developed in the ends of the frame beams with the occurrence of ultimate connection capacity. When the cyclic displacement increased to $5\Delta_y$, the ring beam experienced concrete spalling in the vicinity of frame beam, with the formation of lantern-shaped cracks in the ring beam side. The reinforcements in the region of the plastic hinge were exposed. Fig. 8 shows failure modes for the J6-E-B specimen.

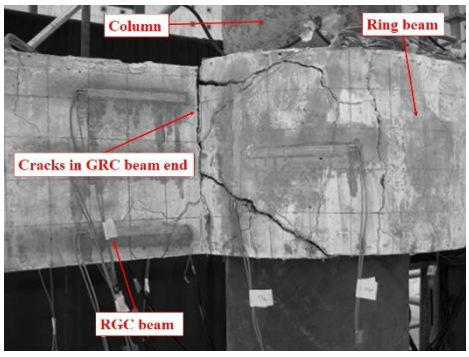

(a) Front side

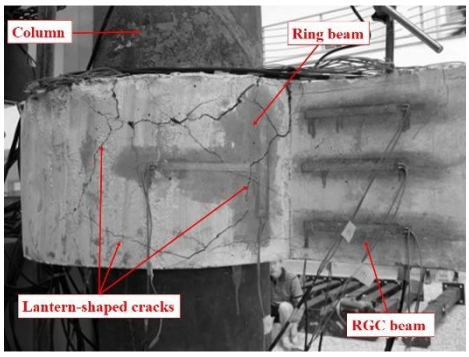

(b) Back side

Fig. 8 Failure mode for JH-E-B connection

3. Finite element model

3.1. Material constitutive model

3.1.1. Concrete

The concrete behavior under cyclic loading was modeled using the ABAQUS concrete plastic damage model, which is capable of simulating stiffness and strength degradation [20]. The core gangue concrete filled in tube was subjected to three-dimensional compressive stress due to tube confinement effect. The response of the confined coal-gangue concrete was simulated using the constitutive model for light-aggregate concrete filled steel tube provided by Fu, as shown in Eq (1).

$$\sigma = \sigma_0 \left[A\left(\frac{\varepsilon}{\varepsilon_0}\right) - B\left(\frac{\varepsilon}{\varepsilon_0}\right)^2 \right] \qquad (\varepsilon \le \varepsilon_0) \tag{1-a}$$

$$\sigma = \begin{cases} \sigma_0 (1-q) + \sigma_0 q \left(\dfrac{\varepsilon}{\varepsilon_0}\right)^{0.1\xi} & [\xi \ge 1.22] \\ \sigma_0 \left(\dfrac{\varepsilon}{\varepsilon_0}\right) \dfrac{1}{\beta\left(\dfrac{\varepsilon}{\varepsilon_0} - 1\right)^2 + \left(\dfrac{\varepsilon}{\varepsilon_0}\right)} & [\xi < 1.22] \end{cases} \qquad (\varepsilon > \varepsilon_0) \tag{1-b}$$

The details of the constitutive model were provided in the related research study. For the unconfined gangue concrete, a constitutive model of the light aggregate concrete developed by Zhang and Cao [21] was used in this study, as illustrated in Fig. 9. This material model can ensure accurate representation of failure modes obtained in the experimental tests and computation convergence during the simulation.

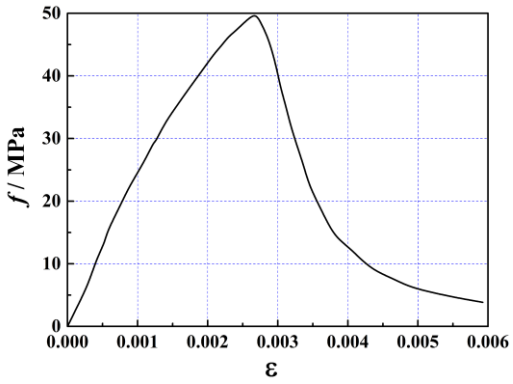

Fig. 9 Constitutive model for unconfined concrete

The concrete damage was represented through the development of the damage variable (d_c), which is in a range from 0 to 1 [22]. The unit of the damage variable indicates the total loss of stiffness and strength in concrete. The concrete damage variable can be calculated using Eq. (2) and incorporated in ABAQUS.

$$d_e = 1 - \frac{\sigma_c + n_c \sigma_{cu}}{E_c\left(\dfrac{n_c \sigma_{cu}}{E_c} + \varepsilon_c\right)} \tag{1}$$

where σ_{cu} is the ultimate compressive stress; σ_c is the compressive stress on the material; E_c is the concrete Yong's modulus; ε_c is the compressive strain; and n_c is the constant factors for compression and should be larger than 0. Based on extensive trials and previous research, n_c is taken to 2 for the confined gangue concrete in GCFST column when subjected to compressive force. n_c was taken to 1 for the unconfined gangue concrete in GC beam. The compressive stiffness recovery factor (w_c) was taken to 0 in the simulations. For the concrete brittle behavior under tension, the fracture energy cracking criterion was used in this model by specifying a fracture energy-cracking displacement curve [23], as illustrated in Eq. (3).

$$G_f = a\left(\frac{f_c'}{10}\right)^{0.7} \times 10^{-3} \quad (3)$$

where a=1.25d_{max}+10; d_{max} represents the maximum coarse aggregate diameter; and f_c' is the gangue concrete compressive strength.

3.1.2. Steel

Given the Bauschinger effects on the composite member response, a kinematic hardening model [24] was employed to represent the steel constitutive model of tube, as shown in Fig. 10. This model was incorporated with an plastic flow rule using a von Mises yield surface. Based on computation trials, the cyclic response of the reinforcement embedded in the concrete was modeled using a double linear model (USTEEL02) [25] developed by Tsinghua University to ensure computation convergence and accurate simulation results. This model (USTEEL02) demonstrates its ability to consider the deterioration of steel capacity for the hysteretic response and provide a reasonable representation of bond slip [26].

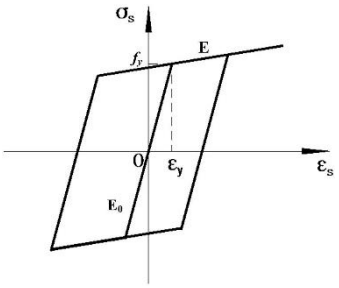

Fig. 10 Constitutive model for steel

3.2. Element formuation and contact model

The coal-gangue concrete and the rigid plates that were placed at the top and base of the GCFST column were modeled using an 8-node, reduced-integration, solid element (C3D8R). A 4-node, continuous, reduced-integration, shell element (S4R) was employed to create steel tube [23]. A truss element was used to model reinforcements embedded in RGC beams. A constraint-based coupling was used to develop the contact between the reinforcement and its surrounding concrete using embedded region constraints in ABAQUS. Fig. 11 shows the ring-beam connection model. The accuracy of finite element model depends on the proper mesh density. The mesh size for the core part of the connection was refined with the increased mesh density for other parts. The mesh sizes of steel tube and confinded coal-gangue concrete were identical to make computation convergence easy.

The tube-to-concrete contact consists of the tangential bond-slip interation and the normal contact [27]. For this model, the tube-concrete bond-slip was modeled using Mohr-Coulomb friction model [23], and the tangential force was determined with a frictional coefficient was 0.6 using a penalty friction approach [28]. The normal contact behavior was simulated using ABAQUS's hard contact to fully transfer the interfacial stresses. In the experimental tests, two hinges were set at both column ends. The plate at the column end was assumed to be rigid in the model. The Poisson's ratio of the rigid plate was 0.0001 and the plate Yong's modulus 1×10^9 GPa. The contact between the plate and the tube was modeled using a shell-to-solid coupling model, and the core concrete-plate contact was simulated using the hard contact model. The cyclic load in the form of displacement was applied on the beam ends as shown in Fig. 11. To replicate experimental boundary conditions, all translations and rotations in X and Z axes were constrained at the column bottom. At the column top, X and Z axes rotations and X and Y axes translations were constrained to model the hinged boundary condition.

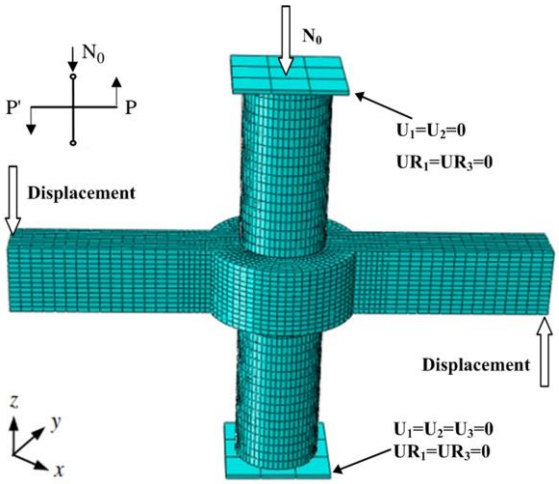

Fig. 11 Finie element model of ring-beam connection

3.3. FE model validation

3.3.1. Failure mode

A comparison of failure modes for the ring beam connection between finite element analyses and experimental tests was illustrated in Fig. 12. It was concluded that modeled failure modes achieved an acceptable agreement with tested modes. The ring-beam connection was damaged by the failure of RGC beams in the vicinity of ring beam, which matched well with experimental results. Experimental results identified that the lantern-shaped cracks were formed at ring beam side, which were observed in finite element models. In the experimental tests and finite element models, the GCFST column did not experience obvious damage. The ring beam connection to GCFST column was shown to exhibit adequate stiffness and strength against the cyclic loads. This finding satisfied the design philosophy in the seismic design code that mandates "strong column and week beam, strong connection and week members" [16].

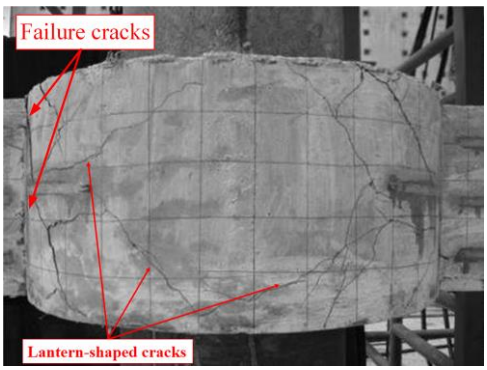

(a) Experiemntal observation

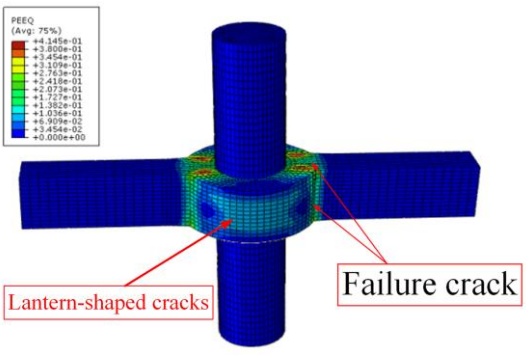

(b) Numerical results

Fig. 12 Finie element model of ring-beam connection

3.3.2. Load-displacement hysteretic curve

Fig. 13 illustrates a comparison of load (P) - displacement (Δ) curves for the ring beam connection between finite element models and experiment tests. P represents the load applied on both beam ends, and Δ is the frame beam deformation. The simulated P - Δ curve for the connection matched with the experimental curve in the terms of load, strength and stiffness degradation, and deformation. It was clear from Fig. 13 that, the stiffness degradation of ring beam connection in finite element analyses was close to those in experimental tests, and modeled strengths during the process of unloading and reloading were almost same with experimental values. The experimental curve was shown to have an obvious pinching shape, while modeled curve was relatively fuller than experimental curves. The shape of modeled curve was slightly different from experimental curve. The difference in curve shape would be caused by the deficiency of selected concrete constitutive model in simulating the large bond-slip between the reinforcements and surrounding concrete. Few research studies have been investigated on the constitutive model of the gangue concrete; therefore, a perfect concrete model was not located in the open literature. The simulated load-bearing capacity, deformation, and the strength and stiffness degradation agreed well with the tested resutls. Overall, the modeled curve obtained in simulations showed acceptable agreements with experimental curve. These FE model for the ring-beam connection were conservative but applicable to complete the research content and purpose.

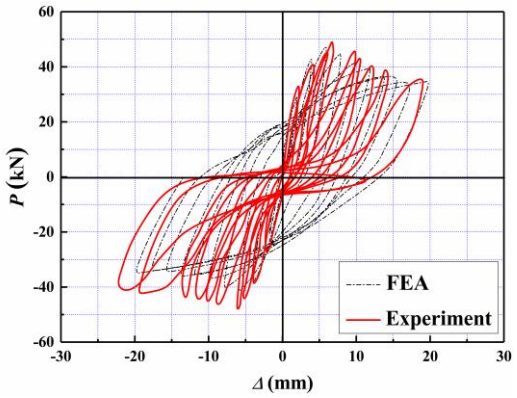

Fig. 13 Expeiremntal and simulated load-displacement curves

3.3.3. Skeleton curve

Fig. 14 compares the modeled and experimental skeleton curves for the ring-beam connection. The skeleton curve of the connection obtained in numerical simulation agreed well with experimental curve, with modeled peak value 10 % less than the recorded bearing capacity. Before the peak values, the modeled curve was identical with experimental curve. Again, the difference was due to the concrete model and simplified simulation of welding for various compnents. Overall, the developed numerical model provided conservative but acceptable predictions on failure mode and load-deformation response for the ring-beam connection under resverse cyclic loading.

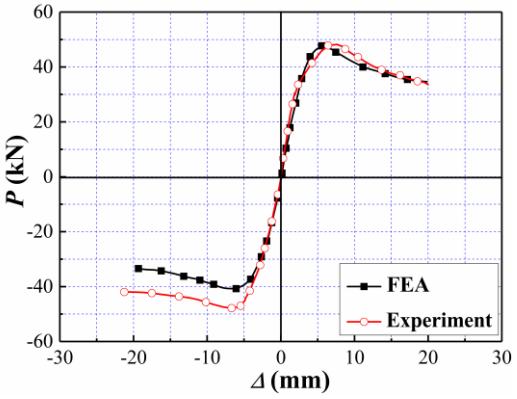

Fig. 14 Comparison of expeiremntal and simulated skeleton curves

The influences of axial load ratio on the ring beam connection behavior were analyzed with the variation of axial loads using the validated model. In this research study, finite element models with the different axial load levels were developed using the interior connection with two frame beams. In models of JH6-A-0.2 and JH6-A-0.8, the axial load was changed to develop additional models with n = 0.2 and 0.8, respectively. Table 3 lists the geometries and design detailing for the developed models.

Table 3
Geometries and design details for developed models

Specimen	$D\times t$ (mm)	H (m)	L (m)	b (m)	h (m)	A_{sf}	b' (m)	A_{sr}	hoop	n
JH-A-B	325×6	1.5	1	0.18	0.25	2Φ20	0.12	2Φ12	Φ10	0.6
JH-A-Z	325×6	1.5	2	0.18	0.25	2Φ20	0.12	2Φ12	Φ10	0.6
JH-A-0.2	325×6	1.5	2	0.18	0.25	2Φ20	0.12	2Φ12	Φ10	0.2
JH-A-0.2	325×6	1.5	2	0.18	0.25	2Φ20	0.12	2Φ12	Φ10	0.8

4. Analysis and results

4.1. Load bearing capacity

A standard method to determine yield point and failure load for the ring-beam connection has not been proposed in the open literature. The method used in the code JGJ/T101-2015 [19] for calculations of the yield strength and corresponding displacement in concrete members was selected for current study. Fig. 15 plots a typical P - Δ skeleton curve of the ring-beam connection. Point A is defined as initial yielding of the connection under cyclic loading. The connection initial yielding was found on the RGC beam. The displacement corresponds to the yield load (P_y) and is defined as the yield displacement (Δ_y). In the connection specimens, P_y approximates to the yield strength of longitudinal reinforcement embedded in the RGC beam. The peak load is the ultimate load (P_{max}) for the connetion at the peak point (B), with the appearance of the ultimate displacement (Δ_{max}). The connection failed at 85% of ultimate load (P_u = 0.85P_{max}), referenced as to the failure load at the point C, with a failure displacement (Δ_u).

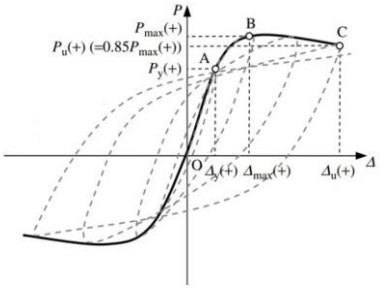

Fig. 15 Typical P-Δ skeleton curve for column-beam connection

Fig. 16 shows the load-displacement curves for these connection models. Table 4 lists critical loads and displacements for the ring-beam connection at points A, B, and C. It was concluded that, (1) Predicted bearing capacities at each stage obtained in finite element analyses were approximately 10% lower than experimental results. Before the ultimate bearing capacity, predicted displacements and loads were close to measured values in experimental tests. After the peak, predicted results were slightly less than the experimental results with the acceptable differences. (2) With an increase in the axial load magnitude, the connection ultimate capacity at n = 0.8 was 18.5% higher than that at n = 0.2 and was 1.1 times that at n = 0.6. The increase in the axial load magnitude at the column top provided a contribution to improving load-bearing capacity of the ring-beam connection. (3) For both experimental testing and numerical modeling, the yield strength, ultimate bearing capacity, and failure load of an exterior connection were larger than those of an interior connection. The exterior connection experienced more severe damage to RGC beam than the interior connection. (4) Overall, all critical displacements and loads were improved as the axial load magnitude increased. After the peak capacity, a higher decrease was shown in the bearing capacity of a connection when subjected to a larger axial load magnitude, and therefore the axial load level for a composite connection needed to be controlled in a reasonable range.

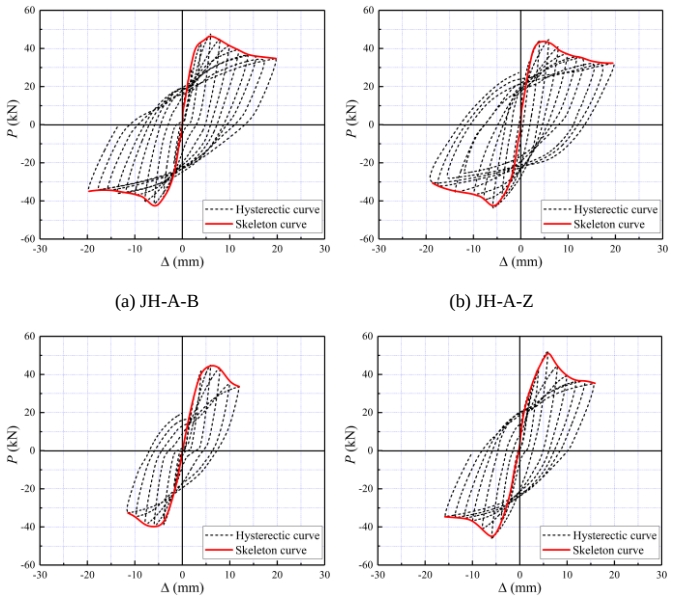

(a) JH-A-B (b) JH-A-Z

(c) JH-A-0.2 (d) JH-A-0.8

Fig. 16 Load-displacement curves for numerical connection models

Table 4
Ctcial loads and displacements at characteristic points

Specimen	N_0 (kN)	n	P_y (kN)	Δ_y (mm)	P_{max} (kN)	Δ_{max} (mm)	P_u (kN)	Δ_u (mm)
JH6-E-B	1800	0.6	21	1.9	39	6.2	32.7	11.4
JH6-E-Z	1800	0.6	24	2.1	49	6.4	42.6	12.7
JH6-A-B	1800	0.6	19	1.8	44.2	5.93	37.5	10.9
JH6-A-Z	1800	0.6	23.4	2.0	47.7	5.95	40.6	11.9
JH6-A-0.2	600	0.2	22.4	1.7	44.2	5.94	37.5	10.6
JH6-A-0.8	2500	0.8	29.4	2.2	52.5	6.0	44.6	11.6

4.2. Degradation of connection strength

The strength degradation of a column-to-beam connection is evaluated using a strength degradation coefficient [24]. The coefficient curve could be used to reflect the decrease of the load during testing and represent the characteristics of strength degradation for the ring-beam connection. The strength degradation coefficient for the column-to-beam conenction is calculated using Eq. (3).

$$\lambda_j = \frac{P_j}{P_{\max}} \tag{3}$$

where λ_j is the strength degradation of ring beam at total loads; P_j is the maximum load at the jth cycles when Δ/Δ_y at beam ends is j; and $P_{\max}$ is the ultimate connection capacity during the whole process of testing.

Fig. 17 illustrates the λ_j - Δ/Δ_y curves for the ring-beam connection. Fig. 17 indicates that, (1) Modeled curves matched well with tested results with respect to the changing trends and values, with the peak value 5% lower than experimental results. (2) After the connection reached its ultimate bearing capacity, a relatively long horizontal part was observed in the coefficient curve. The ring-beam connection possessed a large residual capacity to resist the cyclic loads after the connection experienced its failure load. The ring-beam connection exhibits desirable seismic performance for a building. (3) The strength degradation coefficient (λ_j) increased with the increas in the relative beam displacement when Δ/Δ_y was less than 3. As the relative beam displacement was larger than 3, the strength degradation coefficient began to decreasing. (4) An obvious strength degradation was shown to a connection with a higher axial load ratio. After the peak load, the strength degradation coefficient of the connection specimen was significantly reduced with the increased axial load magnitude.

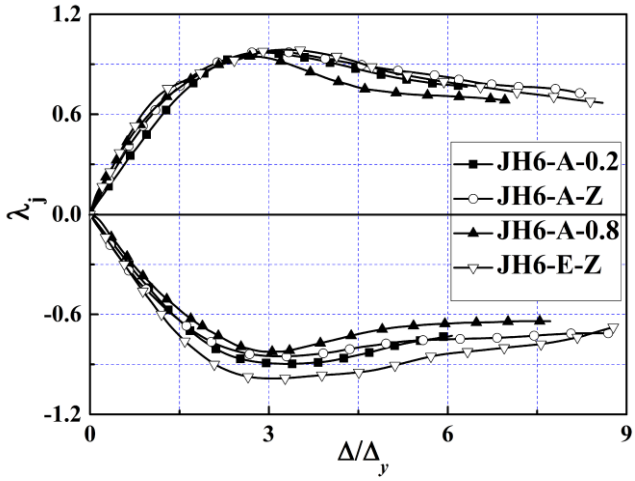

Fig. 17 Strength degradation curves for ring-beam connection

4.3. Degradation of connection stiffness

The concrete cumulative damage during cyclic loading would lead to the stiffness degradation of a column-beam connection [24]. The connection stiffness is defined in terms of maximum load and corresponding displacement at each loading cycle as expressed in Eq. (4).

$$K_j = \frac{\sum_{i=1}^{n} P_j^i}{\sum_{i=1}^{n} u_j^i} \tag{4}$$

where K_j is the stiffness of the column-beam connection; P^i_j is peak load at the jth cycle when the Δ/Δ_y in both beam ends is j; and u^i_j as maximum displacement at the jth cycle when Δ/Δ_y in both beam ends is j.

The connection stiffness (K_j) versus relative beam displacement curves are shown in Fig. 18. It was concluded from this figure that the stiffness degeneration of ring-beam connection was relatively slow, identifying its remarkable ability to resist the lateral sway. Furthermore, before the ultimate bearing capacity, the connection stiffness increased with the increased axial load magnitude. After that, the connection stiffness with a higher axial load magnitude reduced more significantly. The ring-beam connection at a higher axial load ratio experienced severer stiffness degeneration. The axial load ratio for the ring-beam connection should be desgined in a reasonable range to avoid an excessive stiffness degradation.

Overall, the ring-beam connection capacity gradually decreased after its ultimate load. The strength and stiffness degradation resulted in the comprosmised capacity of the ring-beam connection under cyclic loading. Primary factors which significantly affected the strength and stiffness degradation for the ring-beam connection included the elastic-plastic property and accumulative damage during cyclic loading. The damage was produced due to the formation and development of concrete cracking. The steel tube confinements on the coal-gangue concrete inhibited the propagation of crack. As a result, the confinement effect improved the strength and stiffness degradation of the ring-beam connection when subjected to cyclic loads.

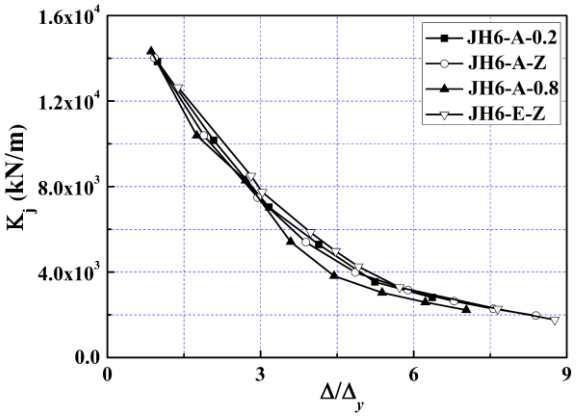

Fig. 18 Stiffness degradation curves for ring-beam connection

4.4. Ductility

The ductility is a physical property of RC structure which identifies its capacity of sustaining large permanent changes in shape. The ductility of a column-beam connection, a vital factor in the earthquake-resistant design, is evaluated using a displacement ductility coefficient [25]. The coefficient of displacement ductility (μ) is calculated using the yield and failure displacements as shown in Eq. (5).

$$\mu = \frac{\Delta_u}{\Delta_y} \tag{5}$$

in which Δ_u is failure displacement; and Δ_y is yield displacement. An angular ductility coefficient is used to evaluate the connection ductility, which is determined using yield and failure angular displacement, as shown in Eq. (6).

$$\mu_0 = \frac{\theta_u}{\theta_y} \tag{6}$$

where μ_0 is the angular displacement ductility coefficient; θ_y and θ_u is the yield and failure angular displacement, respectively. The displacement angle of the ring-beam connection (θ) can be calculated from $\theta = \arctan(\Delta/H)$ according to the code GB50011-2010 [16], in which H is the column height. Table 5 summarizes the tested and simulated ductility coefficients.

Table 5
Displacement and angular ductility coefficient

Specimen	n	Δ_y (mm)	Δ_u (mm)	μ	θ_y (rad)	θ_u (rad)	μ_0
JH6-E-B	0.6	1.9	11.4	6.0	0.0013	0.0076	5.98
JH6-E-Z	0.6	2.1	12.7	6.1	0.0014	0.0085	6.04
JH6-A-B	0.6	1.83	10.9	6.0	0.0012	0.0073	5.95
JH6-A-Z	0.6	2.02	11.9	5.9	0.0014	0.0079	5.87
JH6-A-0.2	0.2	1.75	10.6	6.1	0.0012	0.0071	6.04
JH6-A-0.8	0.8	2.21	11.6	5.3	0.0015	0.0077	5.24

It was observed from Table 5 that, (1) The displacement ductility coefficients of studied connections ranged from 5.0 to 6.1, which satisfied the principle that μ ≥ 3 for the RC structural components. (2) For the high-rise buildings, the design code GB50011-2010 [16] mandated the ductility limit, including an elastic angular displacement limit of 0.0033 rad, and an elastic-plastic angular displacement limit of 0.02 rad. According to Table 5, all angle displacement ductility coefficients of these studied connections satisfied requirements in the code. Results indicated that the ring-beam connection that connected the RGC beams and GCFST columns exhibited high ductility in a seismic event. (3) The ductility of the ring-beam connection slightly reduced as the axial load magnitude increased, as shown in Fig. 19. The influence of the axial load ratio was relatively insignificant to the ductility of the ring-beam connection.

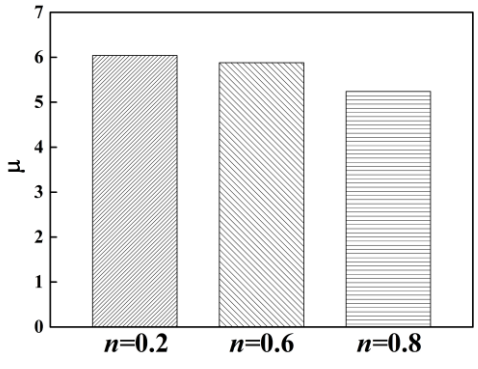

Fig. 19 Effect of axial load ratio on connection ductility

4.5. Energy dissipation

An equivalent damping coefficient and an energy dissipation coefficient recommended in JGJ/T101-2015 [19] were used to analyze the energy dissipation ability of the ring-beam connection that connected the RGC beams and GCFST columns in this study. An equivalent damping coefficient (h_e) is formulated in Eq. (7) and shown in Fig. 20.

$$h_e = \frac{1}{2\pi}\frac{S_{ABD} + S_{BCD}}{S_{OAE} + S_{OCF}} \tag{6}$$

where S_{ABD}, S_{BCD}, S_{OAE}, and S_{OCF} are areas below the corresponding curves ABD, BCD, OAE and OCF, respectively. The energy dissipation coefficient (E_{dc}) is a ratio of the total energy in a hysteretic loop to the elastic energy of the column-beam connection and calculated using $E_{dc} = 2\times\pi\times h_e$.

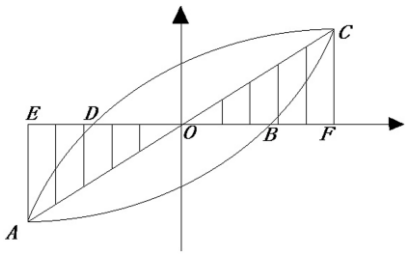

Fig. 20 Stiffness degradation curves for ring-beam connection

Table 6 lists the coefficients for the tested ring-beam connections. It was observed that the equivalent damping coefficients of all studied connections were ranged from 0.20 to 0.25. Based on the related research studies [25], the average equivalent damping coefficients were determined to 0.1 for a normal RC connection and 0.3 for a steel rigid connection. The equivalent damping coefficients of these tested connection specimens were better than the traditional RC connection, and less than the steel rigid connection. As the axial load ratio increased, the energy dissipation capacity of ring-beam connection between GCFST column and RGC beam was improved, and axial load ratio should be controlled within a reasonable range to ensure its desirable energy dissipation capacity in a seismic event. The energy dissipation coefficients of the studied ring-beam connections satisfied requirements in the seismic design code.

Table 6
Equivalent damaping coefficient for studied connections

	Specimen	n	h_e	E
Tests	JH6-E-B	0.6	0.20	1.23
	JH6-E-Z	0.6	0.25	1.57

5. Parametric studies

Parametric analysis was executed to examine the effects of material and structural parameter on the ring-beam connection response to quasi-static loads. The parameters considered in this study included: (i) axial load ratio (n); (ii) column steel ratio (α); (iii) ring beam width (b_0); (iv) confined concrete strength ($f'_{c,c}$); (vi) column slenderness ratio (λ); and (vii) column-beam stiffness ratio;); and (v) unconfined concrete strength ($f'_{c,b}$). Fig. 21 shows the results of the parametric studies, in which JH6-A-Z was used as the baseline model.

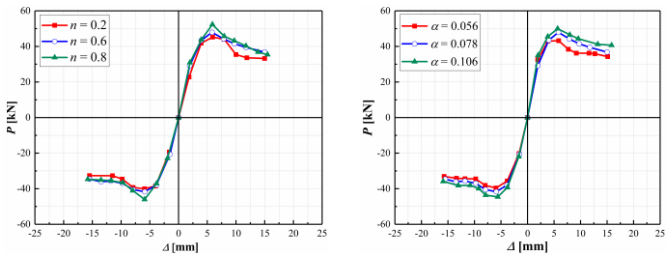

(a) axial load ratio (b) column steel ratio

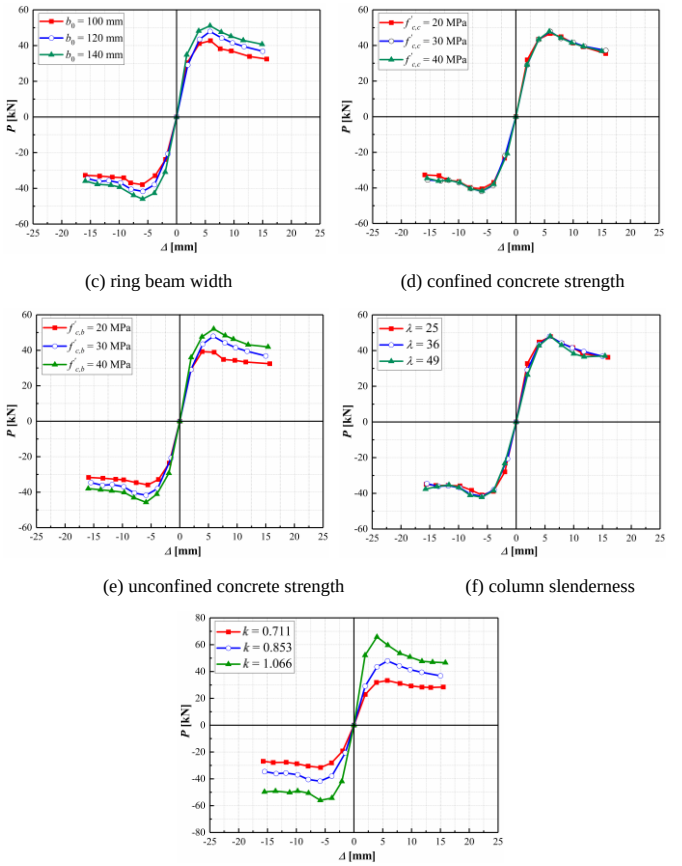

Fig. 21 Skeletion curves with effects of studied parameters

Fig. 21 (a) illustrates that, as the axial load ration increased, the load-bearing capacity of the ring-beam connection was improved. The peak load for the connection at n = 0.8 was 10.1% and 18.8% higher than that at n = 0.6 and 0.2, respectively. The increase in the preload magnitude at the top of the GCFST column resulted in the improved bending strength of the column, which contributes to the increased resistance and capacity of the ring-beam connection.

Fig. 21 (b) shows that the increase in column steel ratio led to the improvement in the connection load-bearing capacity. The peak load for the connection was increased by 11% and 4% when λ increased from 0.056 to 0.078 and from 0.078 to 0.106, respectively. The strength of the confined concrete was improved with the increased tube confinement as the steel ratio increased, resulting in the enhanced load-bearing capacity of the ring-beam connection.

Fig. 21 (c) indicates that the increase in the ring beam width resulted in the improvement of the ring-beam connection capacity. When the width increased from 100 mm to 140 mm, the peak load was improved by 19.7%. A reasonable increase in the width of the circular ring beam improves its ability to transfer internal forces to the GCFST column, which contributes to the capacity resistance of the ring-beam connection.

It was observed from Fig. 21 (d) and (f) that the influences of confined concrete strength and the column slenderness ratio were insignificant for the connection behaviors. The ring-beam connection was designed in accordance with the specifications of current codes in which the beam should be weaker than the column in the earthquake event with the intact column. Thus, the connection behavior did not significantly change with the variations of the confined concrete strength and column slenderness ratio.

Fig. 21 (e) shows that the connection capacity was improved when the unconfined concrete strength in the beam increased. The peak load for the connection with $f'_{c,b}$ = 40 MPa was 8.6% and 32.6% higher than that for $f'_{c,b}$ = 30 MPa and $f'_{c,b}$ = 20 MPa, respectively. The connection with the higher strength unconfined concrete would possess larger resistance against cyclic loads with the formation of cracks. It was seen from Fig. 21 (g) that the connection capacity was enhanced when the column-beam stiffness ratio increased. The peak load was improved by 43.8% with the increase of k from 0.771 to 0.853, and the peak load increased by 37.4% when k increased from 0.853 to 1.066.

6. Development of restoring force model

For the design purpose, seismic behavior of structural components and system can be theoretically examined using a restoring force model. The restoring force model of a structural component represents the theoretical relation between the restoring force and the deformation, which can demonstrate the structural response in the seismic event including the load-bearing capacity, degradation of strength and stiffness, ability to dissipate energy, and deformation resistance. Numerical results in parametric studies were used to derive the restoring force model of skeleton curve for the ring-beam connection to GCFST column. The maximum load-bearing capacity (P_m) and its corresponding deformation (Δ_m) were utilized as the refence point in the study to simply the comparison and development of theoretical equation. The skeleton curves of the connections considering effects of various parameters were normalized by the reference strength and deflection, as illustrated in Fig. 22, in which the skeleton curves for various connections exhibited the similar trend involving three distinct segments: linear elastic stage, plastic-hardening stage, and reducing stage.

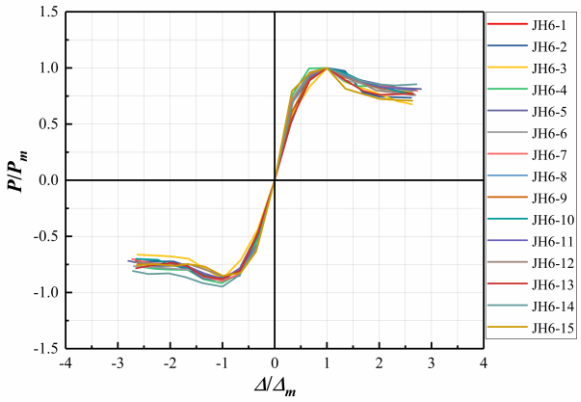

Fig. 22 Normalized skeleton curves for ring-beam connection

Based on the observations and related studies, a three-fold multilinear model was used to represent the restoring force model of skeleton curve for the cyclic-loaded ring-beam connection between the RGC beams and GCFST column. The regression analysis of numerical results from parametric studies was conducted to determine the three-fold multilinear model with the characteristic points, as illustrated in Fig. 23. According to the reference point, the $P/P_m - \Delta/\Delta_m$ interaction relation with six linear segments was developed, as shown in Eqs. (7) – (8).

(a) OABC stage

$$\frac{P}{P_m}=\begin{cases}2.2\times\dfrac{\Delta}{\Delta_m} & \text{OA segement}\\ 0.53\times\dfrac{\Delta}{\Delta_m}+0.51 & \text{AB segment}\\ 1.24-0.2\times\dfrac{\Delta}{\Delta_m} & \text{BC segment}\end{cases} \tag{7}$$

(b) OA′B′C′ stage

$$\frac{P}{P_m}=\begin{cases}1.8\times\dfrac{\Delta}{\Delta_m} & \text{OA}'\text{ segement}\\ 0.52\times\dfrac{\Delta}{\Delta_m}-0.38 & \text{A}'\text{B}'\text{ segment}\\ -0.98-0.09\times\dfrac{\Delta}{\Delta_m} & \text{B}'\text{C}'\text{ segment}\end{cases} \tag{8}$$

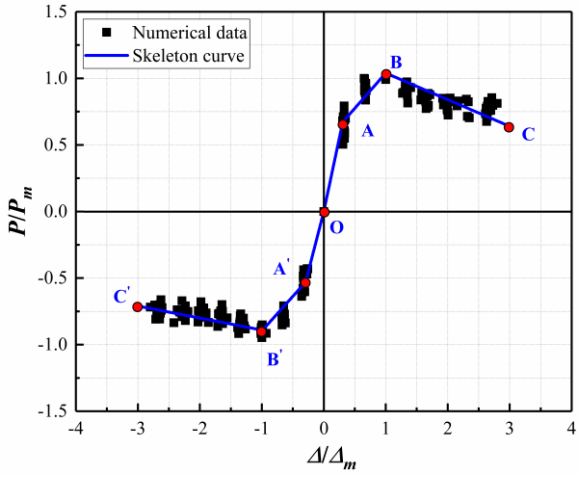

Fig. 23 Restoring force model of skeleton curves

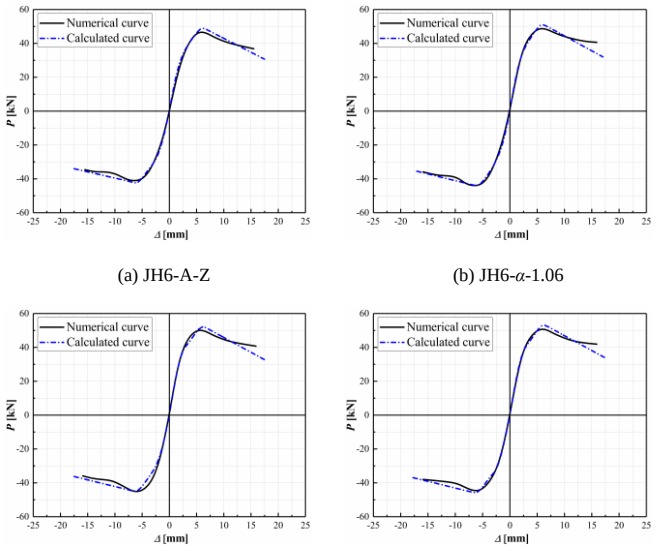

(a) JH6-A-Z (b) JH6-α-1.06

(c) JH6-b_0-1.06 (b) JH6-$f'_{c,b}$ -40

Fig. 24 Comparison of numerical and calculated skeleton curves

The developed three-fold multilinear model is useful to predict the restoring force model of skeleton curve for the ring-beam connection between RGC beams and GCFST column using the ultimate capacity and corresponding deformation when subjected to the cyclic loads. Fig. 24 compares the predicted and numerical skeleton curves for several cases. As shown in Fig. 24, the predicted skeleton curves reasonably matched with numerical results, indicating the feasibility of the developed restoring force model for the ring-beam connection. The comparison results also demonstrated the ability of the developed model to represent the deformation-cyclic load interactions for the ring-beam connection, which provides application and design suggestions of this composite connection for engineering applications.

7. Conclusions

This study conducted investigations that investigated seismic behavior of the ring-beam connection that connected the RGC beams to the GCFST column. Several behavioral indexes were examined to evalute its performance in the seismic event. The conclusions were obtained:

• The ring-beam connection that connected RGC beams to GCFST column with the full spindle-shaped hysteretic curve exhibits reasonable strength and stiffness degradation. The ring-beam connection failed with the development of a plastic hinge in RGC beam, which satisfied the requirements of the design principles that “strong column and week beams”. The ring-beam connection exhibited acceptable seismic behaviors.

• The displacement ductility coefficient for the studied ring-beam connections were higher than 5, which satisfies the seismic design requirement that the displacement ductility coefficient should be higher than 3. The angle displacement ductility coefficients of examined ring-beam connections also were larger than the required limit in the code. The equivalent damping coefficient of ring-beam connection was in a range of 0.1~0.3, which is higher than that obtained from normal RC component. The study results showed that the ring-beam connection between RGC beams and GCFST column could be effectively applied in the seismic regions.

• Detailed parametric studies indicated that the ring-beam connection seismic behaivor was significantly affected by steel ratio, ring beam width, unconfined concrete strength, and column-beam stiffness ratio. The load-bearing capacity of the ring-beam connection was improved as the steel ratio, unconfined concrete strength for the RGC beam, ring beam width, and column-beam stiffness ratio increased. The effects of the confined concrete strength and column slenderness ratio were insignificant to the connection resistance due to the seismic design fundamentals.

• A restoring force model of skeleton curve for the ring-beam connection that connected the RGC beams to the GCFST columns was developed using a three-fold multilinear model through regression analysis. The accuracy of the developed three-fold multilinear model was also validated by comparing with simulated results. This restoring force model effectively represents the load-deformation interaction relation for the ring beam connection under cyclic loading.

Acknowledgments

The authors would like to acknowledge supports for this research from the Key Projects of National Natural Science Foundation of China, China (51938009), National Natural Science Foundation of China, China (51878419) and (51578345), Natural Science Foundation of Jiangsu Province (BK20200996), and China Postdoctoral Science Foundation (2020M681566).

References

[1] Li G., Fang C., An Y., and Zhao X. (2015). "Seismic Behavior of Rebar-Penetrated Joint between GCFST Column and RGC Beam." Steel and Composite Structures, 19(3), 547-567.
[2] AL-Eliwi B.J., Ekmekyapar T., Faraj R.H., Gogus M.T., and AL-Shaar A.A. (2017). "Performance of lightweight aggregate and self-compacted concrete-filled steel tube columns." Steel and Composite Structures, 25(3), 299-314.
[3] Yu X., Tao Z., and Song T.-Y. (2016). "Effect of different types of aggregates on the performance of concrete-filled steel tubular stub columns." Materials and Structures, 49(9), 3591-3605.
[4] Li G.C., and Zhong S.T. (2002). "Strength and Lateral Deformation Coefficient of Gangue Concrete Restrained by Steel Tube." Harbin Jianzhu Daxue Xuebao/Journal of the Harbin University of Civil Engineering and Architecture, 35(3), 20-23.
[5] Nelson A.J., Rakau O., and Dörrenberg P. (2010). "Green Buildings: A Niche Becomes Mainstream."
[6] Wang C.L., Ni W., Zhang S.Q., Wang S., Gai G.S., and Wang W.K. (2016). "Preparation and properties of autoclaved aerated concrete using coal gangue and iron ore tailings." Construction and Building Materials, 104, 109-115.
[7] Miller D.K. (1998). "Lessons learned from the Northridge earthquake." Engineering Structures, 20(4), 249-260.
[8] Zhao B., Taucer F., and Rossetto T. (2009). "Field Investigation on the Performance of Building Structures during the 12 May 2008 Wenchuan Earthquake in China." Engineering Structures, 31(8), 1707-1723.
[9] Goldsworthy H., and Gardner A. (2006). "Feasibility study for blind-bolted connections to concrete-filled circular steel tubular columns." Structural Engineering and Mechanics, 24(4), 463-478.
[10] Kataoka M.N., and de Cresce El A.L.H. (2015). "Beam–column composite connections under cyclic loading: an experimental study." Materials and Structures, 48(4), 929-946.
[11] Agheshlui H., Goldsworthy H., Gad E., and Mirza O. (2017). "Anchored blind bolted composite connection to a concrete filled steel tubular column." Steel and Composite Structures, 23(1), 115-130.
[12] Tizani W., Wang Z.Y., and Hajirasouliha I. (2013). "Hysteretic performance of a new blind bolted connection to concrete filled columns under cyclic loading: An experimental investigation." Engineering Structures, 46, 535-546.
[13] Khanouki M.A., Sulong N.R., Shariati M., and Tahir M. (2016). "Investigation of through beam connection to concrete filled circular steel tube (CFCST) column." Journal of Constructional Steel Research, 121, 144-162.
[14] Choi S.-M., Park S.-H., Yun Y.-S., and Kim J.-H. (2010). "A study on the seismic performance of concrete-filled square steel tube column-to-beam connections reinforced with asymmetric lower diaphragms." Journal of Constructional Steel Research, 66(7), 962-970.
[15] CECS28-2012 (2013). "Technical Specification for Concrete-Filled Steel Tubular Structures."Beijing, China.
[16] GB50011-2010 (2011). "Code for Seismic Design of Buildings." Chinese Building Press, Beijing, China.
[17] GB/T228-2002 (2003). "Code of Metallic Materials—Tensile Testing at Ambient Temperature."Beijing, China.
[18] GB/T50081-2002 (2003). "Standard for Test Method of Mechanical Properties on Ordinary Concrete."Beijing, China.
[19] JGJ/T101-2015 (2015). "Specification of Testing Methods for Aseismic Property of Building." China Building Industry Press, Beijing, China.
[20] Yu T., Teng J., Wong Y., and Dong S. (2010). "Finite element modeling of confined concrete-II: Plastic-damage model." Engineering structures, 32(3), 680-691.
[21] Zhang J.W., and Cao S.Y. (2009). "Research on the Stress-Strain Curves of Structural Lightweight Aggregate Concrete." Building Science, 24(11), 83-85.
[22] Li W., and Han L.H. (2011). "Seismic Performance of CFST Column to Steel Beam Joints with RC Slab: Analysis " Journal of Constructional Steel Research, 67(1), 127-139.

[23] Sorenson H.K. (2003). "ABAQUS version 6.4: theory manual, users' manual, verification manual and example problems manual." Hibbitt, Karlson, Sorenson Inc. USA.
[24] Han L.H. (2004). "Concrete-filled steel tubular structure-theory and practice." Science Press, Beijing.
[25] Lu X.Z., Ye L.P., and Miu Z.W. (2009). Static-Plastic Analysis on Seismic Performance of Buildings, China Architecture & Industry Press, Beijing, China.
[26] Li G.C., Fang C., Zhao X., An Y.W., and Liu Y. (2015). "Cyclic Behavior of Rebar-Penetrated Connection between Gangue Concrete Filled Steel Tubular Column and Reinforced Gangue Concrete Beam." Advanced Steel Construction, 11(1), 54-72.
[27] Wan C.Y., and Zha X.X. (2016). "Nonlinear analysis and design of concrete-filled dual steel tubular columns under axial loading." Steel and Composite Structures, 20(3), 571-597.
[28] Johnson R.P. (2008). Composite structures of steel and concrete: beams, slabs, columns, and frames for buildings, John Wiley & Sons.